SAND2000-1993C

# Porosity in Stainless Steel LENS Powders and Deposits

D.F. Susan[a], J.D. Puskar[a], J.A. Brooks[b], and C.V. Robino[a]
Sandia National Laboratories
[a]Albuquerque, NM and [b]Livermore, CA



## Abstract

Laser Engineered Net Shaping (LENS) utilizes a laser beam to melt fine powders to produce three-dimensional engineering structures line by line and layer by layer. When building these structures, defects including lack-of-fusion (LOF) at interlayer boundaries and intralayer porosity are sometimes observed. LOF defects can be minimized by adjusting processing parameters, but the sources of intralayer porosity are less apparent. In this paper, the amount and size distributions of 17-4PH and 304L powders and pores within the powder were characterized in parallel with the intralayer porosity in LENS deposits fabricated from the same materials. Intralayer porosity increased with increased powder porosity; but was not well correlated with deposition parameters. The results demonstrate the importance of careful characterization and specification of starting powders on the quality of the final LENS deposits.

---

## Introduction

In the LENS (Laser Engineered Net Shape) process, parts are fabricated by forming a molten pool of material with a laser into which particles are injected [1]. By moving the workpiece, the structure is built line by line into a wide variety of complex geometries. The use of a finely focused laser to form the rapidly traversing pool can produce relatively high solidification velocities and high cooling rates (>$10^3$ °C/sec) through the solidification range. Since the position of the laser is pre-determined from a CAD model, if the deposit is not sufficiently high in relation to the focal point of the laser, it may result in interlayer lack of fusion (LOF). In contrast, the exact cause(s) of spherical, intralayer porosity are not clearly understood. It is possible that gas dissolved or entrapped in the melt may not have sufficient time to escape to the top of the melt pool due to rapid solidification rates. There are many possible sources of the gas, such as surface contamination, entrainment during turbulent impact of particles into the molten pool, contamination by powder-feed gases, gasses contained within the powder, or vaporization of high vapor pressure alloy constituents. Previous work has focused on controlling the size of the melt pool and other parameters to produce good deposit microstructures and eliminate defects such as interlayer LOF [2-6]. This paper will report on the characterization of porosity and its relation to the starting LENS powders.

Powders used in the LENS process are generally gas-atomized. During the atomization process, small pores can be formed within the individual powder particles [7-9]. These voids are most likely produced by entrapment of the atomizing gas (e.g. argon) within the material during initial droplet formation and break-up [7-9]. Atomized powders may contain different amounts of porosity depending on alloy composition, particle size, and atomization conditions used by the producer. However, no work has been done on the effects of starting powder characteristics on the resultant LENS deposits. While LENS processing parameters such as laser power, travel speed, and powder feed rate may have significant influence on void formation, characterization and careful choice of starting powders may also be an important way to control porosity.

## DISCLAIMER

## Experimental Procedure

Two types of stainless steel powders and deposits were investigated: 304L and 17-4PH. Five lots of atomized powder -- one lot of 17-4PH and four lots of 304L (denoted as 304L-1,2,3, and 4) -- were characterized and then used to produce LENS builds. The nominal powder sizes, reported by the manufacturers, were –100/+270 mesh (approximately 50 to 150 μm diameter). Thin-wall 'shell' and three-dimensional 'block' builds (Figure 1) were deposited on stainless steel substrates with the following process parameters: laser power 520 to 700W, powder feed rate 30 to 36 g/min, travel speed 50, 100, and 200 cm/min. The major process variables in this study included starting powder characteristics, laser travel speed, and build geometry. To deposit material with faster travel speeds, the laser power and/or powder feed rate must also be increased to maintain similar heat inputs.

The starting powder morphology was characterized by quantitative image analysis (200 times magnification) to determine powder size and distribution, amount of porosity, and pore size and distribution. Thin-wall deposits were prepared in vertical cross-sections (Figure 1) to show all layers from the substrate to the top of the deposit. Block deposits were also sectioned along the z-axis parallel to the x-axis and, therefore, showed individual layers in both longitudinal (x direction) and transverse (y direction) orientations. Image analysis was performed on as-polished deposits (50 times magnification) to characterize the amount of porosity, pore size, and distribution. Since relatively low magnification was needed to obtain statistically meaningful bulk porosity measurements, very small pores (1-2 μm in diameter) were not included in the analyses.

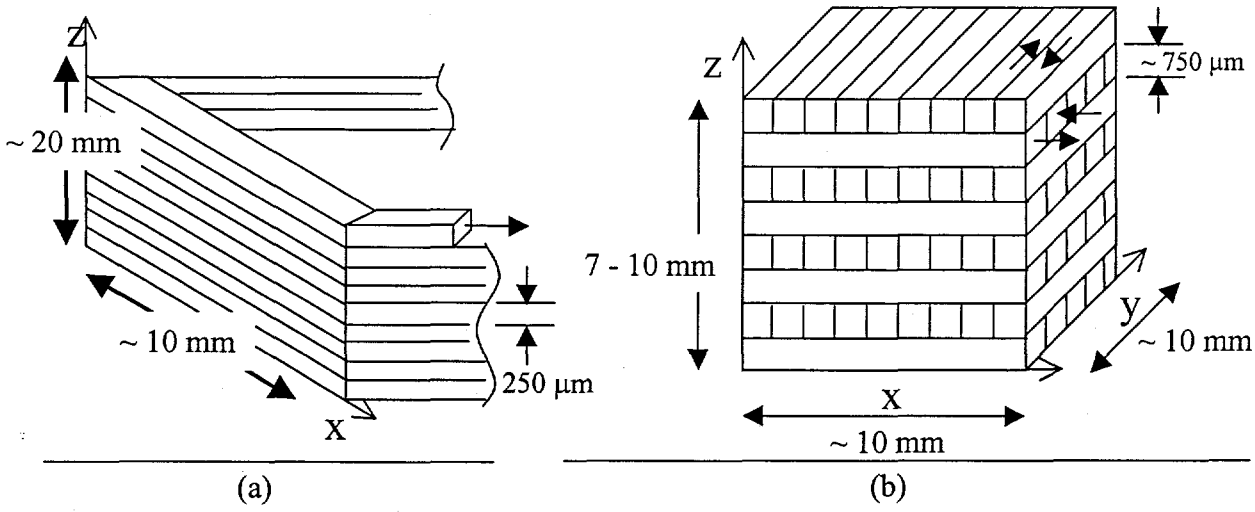


Figure 1. Schematic diagrams of a) shell and b) block LENS builds.

## Results and Discussion

### *Pore Morphology and Deposit Microstructures*

Typical light optical photomicrographs of powders are shown in Figure 2. Particle shape was generally spherical for all lots analyzed. In Figure 2a, the 17-4PH powder is shown which contained a large amount of porosity from the atomization process. The pores within the

particles are also spherical in shape. Based on the pore morphology, it was assumed that pores within the powders contained the atomizing gas, as shown by others [9]. Figure 2b shows sample 304L-4, which contained the lowest amount of porosity for all the lots analyzed. The morphology of typical deposits are displayed in Figure 3. Two types of porosity can be distinguished: interlayer LOF and intralayer (spherical) porosity. Interlayer porosity is caused by lack of fusion between layers, has an elongated shape, and is always found between individual LENS layers (Figure 3a). In contrast, intralayer porosity is spherical and does not appear to be associated with any specific microstructural features (Figures 3b-d). Etching must be performed to positively distinguish between the two types of porosity. However, in some instances spherical pores are located along the interface between layers. It is not clear whether these voids are spherical LOF defects, the remnants of elongated LOF porosity, or caused by some other mechanism. When viewing layers in the transverse orientation (every other layer in the cross-section of a block deposit), it is sometimes difficult to determine the shape of interlayer porosity since it may be elongated normal to the plane of polish. In this study, however, it was possible in most cases to distinguish between the two types of porosity based on shape and location within the deposit. In Figures 3a and b, unmelted or partially melted particles are found within the deposits, as shown previously by Brice et al [5]. It is interesting to note that small voids are found *within the individual particles*. This evidence strongly suggests that particle porosity may directly contribute to deposit porosity.

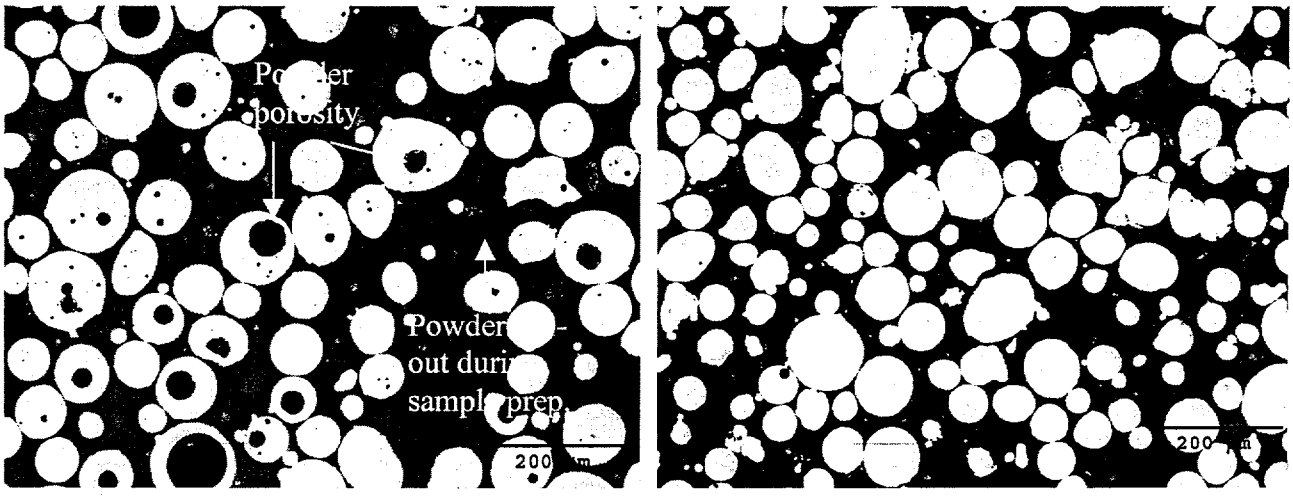


(a) (b)

Figure 2. Photomicrographs of as-polished a) 17-4PH and b) 304L-4 LENS powders.

Typical microstructures of stainless steel LENS deposits are also apparent in Figure 3. In Figures 3a (block samples produced from lot 304L-3), the structure contains mostly austenite, which transformed from delta ferrite on cooling. Only a small amount of the original ferrite is retained, not visible at this magnification. In contrast, 17-4PH deposits (Figure 3b) contain a martensitic structure. It is likely that 17-4PH also solidified as delta ferrite and transformed to austenite and then martensite on cooling. In Figures 3c and d, the block 304L-2 deposit structure is mostly austenite, but contains a different ferrite morphology than 304L-3 (Figure 3a).

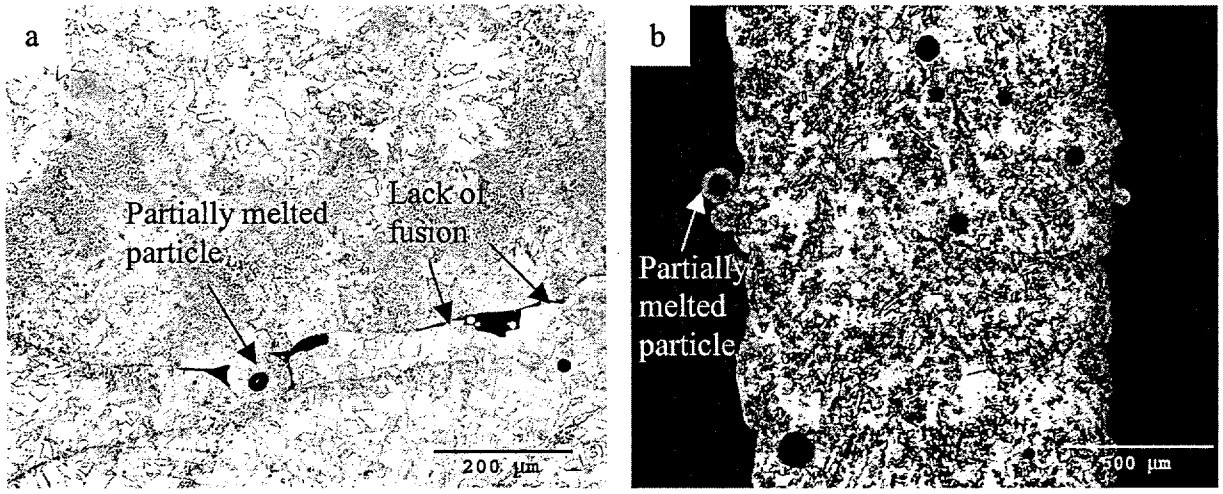


Figure 3. a) Photomicrograph of interlayer lack of fusion in 304L-3, block LENS build. b) Cross-section of 17-4PH, shell build showing spherical porosity.

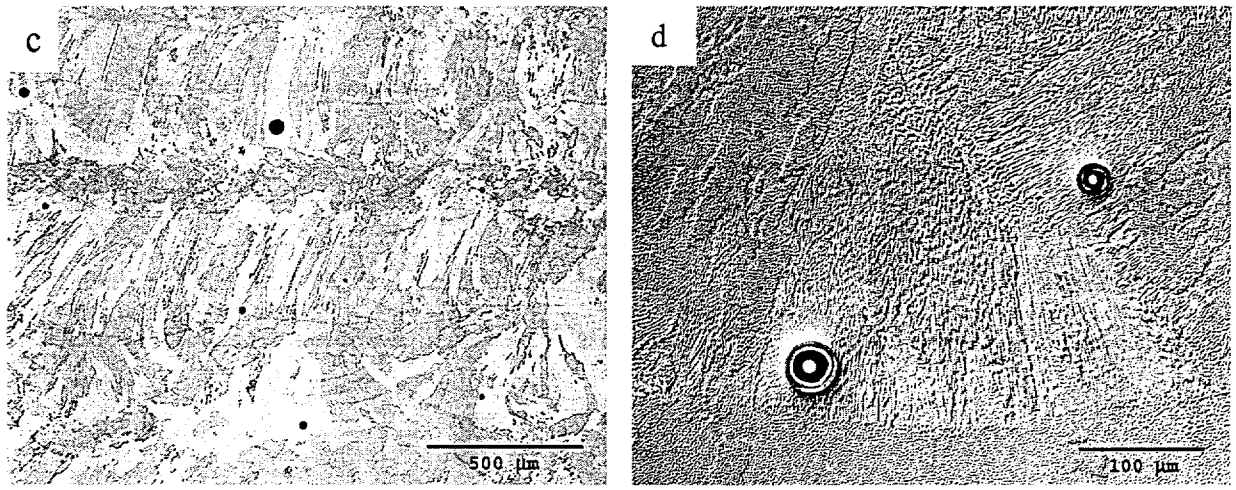


Figure 3. c) Low magnification photomicrograph of spherical porosity in 304L-2, block build. Note smaller size and amount of pores in 304L (Figures 3c) compared to 17-4PH (Figure 3b). d) Higher magnification view of spherical porosity (differential interference contrast).

***Porosity Content***

In block deposits, interlayer (LOF) porosity was most prevalent near the substrate. The LOF near the base of the build is probably related to heat sinking by the substrate during deposition of the initial layers. During deposition, the heat flow conditions change as the deposit effectively becomes pre-heated as more layers are deposited on each other. In thin-wall builds, the voids were spherical and uniformly distributed throughout the deposits and LOF was not observed. Since LOF was generally confined to specific areas in certain deposits and is known to be related to processing parameters, the following analyses only relate to randomly distributed intralayer (spherical) porosity, which is common to all deposits.

Figure 4 exhibits a summary of measured porosity within starting powders and their resultant deposits. In general, the porosity content (based on area % measured by image analysis) in the deposits is lower than in the starting powders. There appears to be a correlation,

however, between the starting powder and the deposits for a given lot of material. For example, lot 304L-4 exhibited the lowest porosity in both powder and deposit while 17-4PH had high powder porosity (about 5 %) and high amounts of porosity in both thin-wall and block deposits. However, the effects governing deposit porosity are likely more complex, possibly depending on details such as the relative size of voids and powder particles. For 304L-1, the porosity in the powder was high (5%) but the shell deposits had only slightly higher porosity than 304L-2 and 304L-3. In block deposits, the 304L-1 porosity was about twice as high as 304L-2 or 304L-3. Possible reasons for the efficient porosity reduction in 304L-1 will be discussed later.

There appeared to be little effect of changing travel speed (50, 100, and 200 cm/min) on porosity in the 304L (shell) deposits, but 17-4PH displayed much higher porosity when deposited at 200 cm/min compared to 100 cm/min, as shown in Figure 4. Overall, the 17-4PH material contained more porosity in both powders and deposits, suggesting a correlation between powder porosity and deposit porosity. However, the correlation is only qualitative since one lot of 17-4PH produced different porosity levels in deposits (1.2 – 4%) depending on processing conditions and build geometry (Figure 4). Also, differences in melt pool geometry and solidification behavior may also affect porosity formation in the two alloy types.

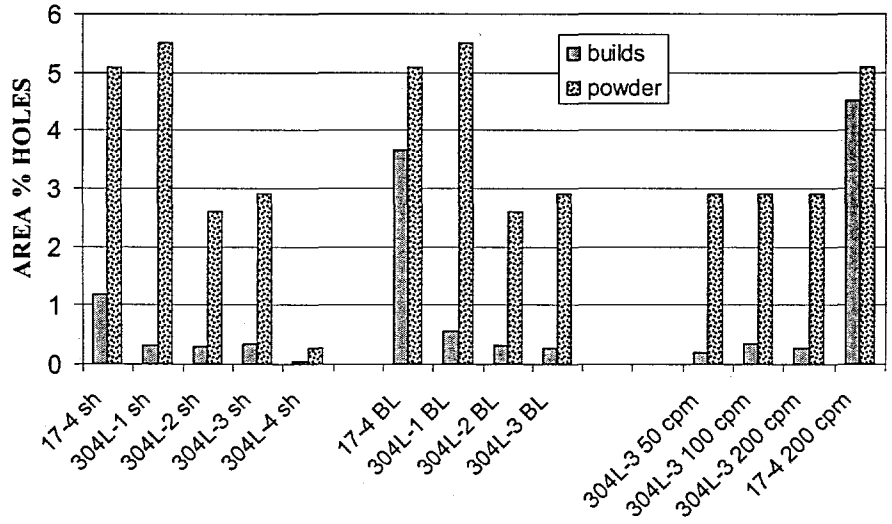


Figure 4. Summary of porosity measurements in powders and LENS builds. Travel speed was 100 cm/min unless otherwise noted. sh = shell, BL = block, cpm = travel speed in cm/min

***Measured Size Distibutions***

*A. Powders and Powder Porosity*

The powder size distributions for each lot were determined using quantitative image analysis and an example of the raw data is shown in Figure 5a as a histogram of particle diameter with 15 equal size intervals. The data represent 10 fields of view at 200 times magnification with a total of 300 to 600 particles analyzed, depending on the particle size in each sample. The data were normalized by total particle area measured. However, when viewing a 2-D cross-section (such as Figure 2), the particles will be intersected at various depths, not always at the center of a particle. The result is an error in favor of smaller particles [9]. For spherical particles, a correction procedure can be applied to the particle size histograms to extract $N_V$, the number of particles per unit volume, from the measured $N_A$, number of particles per area. The procedure involves a matrix correction based on the probabilities that result from random planes sectioning through spheres. The procedure used here is described in Ref (9). The "3-D corrected" data is also shown in Figure 5a. As expected, the relative amounts of particles of a given size are

changed after the correction, since many of the smaller measured particles in the original data are actually sections of larger ones. The procedure was applied to all particle and pore size histograms in this study. However, in most cases the trends in particle size, i.e. the overall shape of the histograms, do not change when the correction is applied. Figure 5b displays histograms for all powder lots. For clarity, the histogram data points for each lot are connected with smooth curves with values on the x-axis representing the centers of the histogram bins. Most of the results appear to follow log-normal behavior which is typical of atomized powders [7]. Using image analysis, the particle size results differ considerably from the manufacturer's reported mesh sizes, with a significant amount of small (< 25 μm diam.) particles. The results also show lots 17-4 and 304L-4 have relatively fewer small particles compared to lots 304L-1,2, and 3.

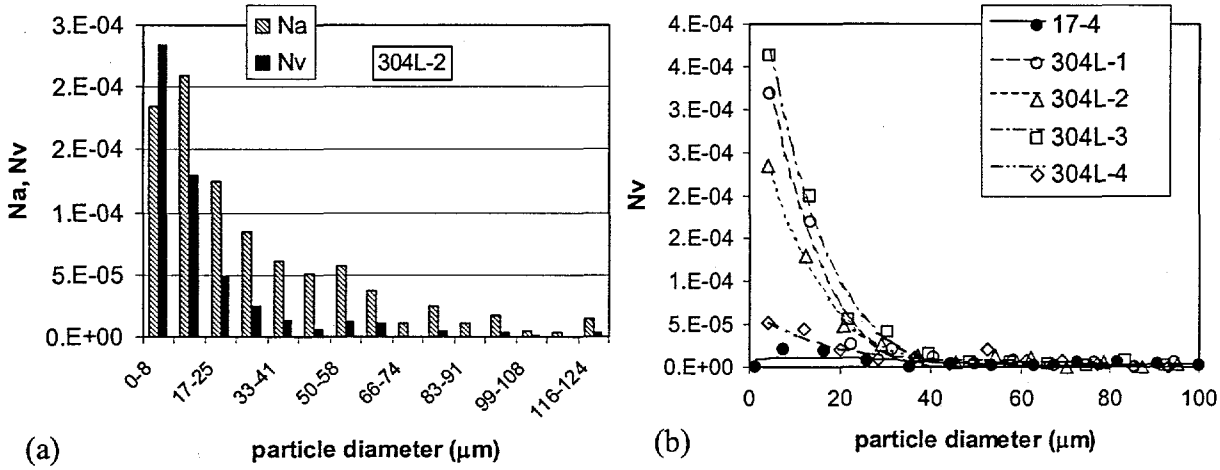


Figure 5. a) Particle size histograms of 304L-2 powder showing $N_A$ (number per area ($\mu m^2$)) and $N_v$ (number per volume ($\mu m^3$)). b) Summary histograms (based on $N_v$).

Figure 6a displays a summary of the histograms of pores within the powders (based on $N_v$). The voids also appear to follow a log-normal relationship with many small voids and a few larger ones. The data was curve-fit using truncated log-normal distributions. For voids within particles, the void sizes must be smaller than the particles in which they are contained. Ratios of average void size (based on spherical geometry) to average particle size are shown in Figure 6b. Although the use of average values gives only a rough estimate of overall powder characteristics, it is evident that there are differences in the size of the voids relative to particle size in these powder lots. In particular, powder lot 304L-1 contains large voids, on average, relative to its particle size.

*B. Porosity in LENS Deposits*

Summary histograms showing pore size distributions in LENS deposits are shown in Figure 7. Distributions for shell and block builds are shown in Figures 7a and b, respectively, and void distributions as a function of travel speed are shown in Figure 7c for shell deposits produced from 304L-3 powder. In Figure 7, the data are from 10 fields of view measured at 50 times magnification on each sample with a total of 80 to 260 voids analyzed, depending on the porosity content of the particular samples. Again, the porosity appears to follow log-normal behavior in most cases. Several observations can be made regarding the void size distributions in Figure 7. First, shell deposits (Figure 7a) produced from 304L-4 powder contain very few

voids compared to the other samples. Second, in block builds (Figure 7b), 304L-1 build displays more voids than 304L-2 and 304L-3. These results can be correlated with Figure 4. It appears that block 304L-1 build contains more small voids (Figure 7b) and porosity content (area %) is twice as high in 304L-1-BL compared to 304L-2-BL and 304L-3-BL (Figure 4). Finally, based on Figures 4 and 7c, a slight broadening of the void size distribution is found with increasing travel speed (304L-3 shell deposits), but no significant change in overall area % porosity.

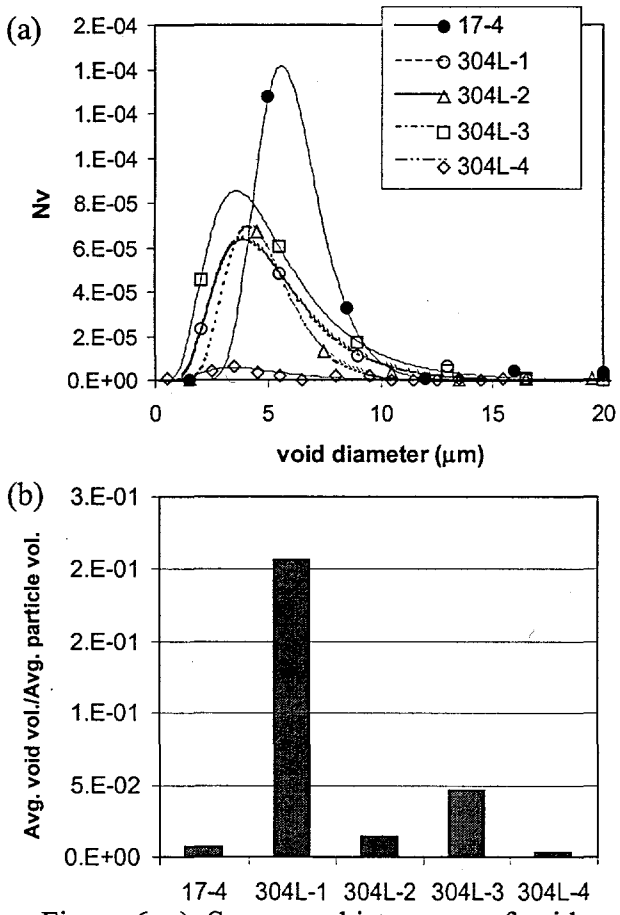


Figure 6. a) Summary histograms of voids within starting LENS powders. b) Ratio of average void volume to average particle volume for LENS powders.

In LENS deposits, the pores are larger than those found in the starting powders. This may indicate that larger pores are formed by accumulation of gas from a number of particles. However, based on the stereological measurements, no obvious quantitative relation could be made between the average void size in the powders and average void size in the deposits. This may be due to other process parameter effects such as entrapment of powder-feed gas during the deposition process.

Based on the results of this study, it appears that deposit porosity is affected by powder porosity. Further, the relative size of voids within the particles may be important. Image analysis results suggest that, for powders with the same starting volume fraction of voids, larger void/particle size ratios tend to result in less porosity. This would explain the efficient reduction in porosity in the 304L-1 deposit. The effect may be due to a mechanism whereby gas escapes from the melt pool surface, since buoyancy increases significantly with gas pore size.

**Conclusions**

Stainless steel LENS powders and deposits were studied using quantitative image analysis to characterize pore size and distribution. Powders, voids within powders, and voids within deposits are spherical in shape and generally follow log-normal size distributions. Starting LENS powders with high porosity content result in deposits with increased porosity. Differences were observed between 17-4 and 304L, with 17-4 having generally higher porosity content in powders and deposits. In addition, powders with large void/particle size ratios may result in less deposit porosity, compared to powders with the same porosity content but lower void/particle size ratios, although this effect may be alloy dependent. Regardless, for a given set of LENS process parameters, powders with the lowest porosity should be specified to minimize LENS deposit porosity.

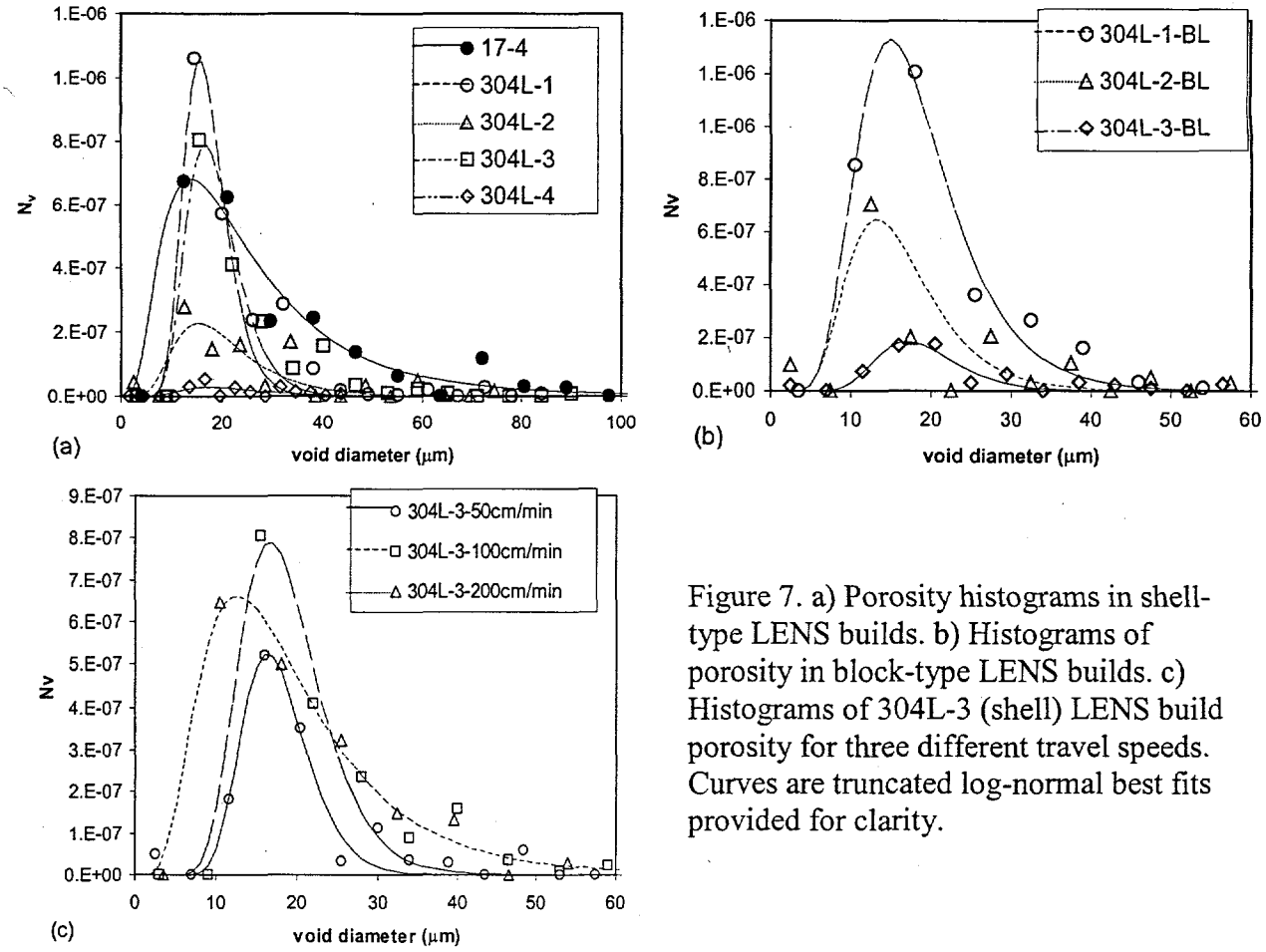


Figure 7. a) Porosity histograms in shell-type LENS builds. b) Histograms of porosity in block-type LENS builds. c) Histograms of 304L-3 (shell) LENS build porosity for three different travel speeds. Curves are truncated log-normal best fits provided for clarity.


## Acknowledgements

The authors would like to thank Mike Oliver for LENS processing, Alice Kilgo for metallography support, and Joe Michael for careful review of the manuscript. Sandia is a multiprogram laboratory operated by Sandia Corporation, a Lockheed Martin Company, for the United States Department of Energy under Contract DE-AC04-94AL85000.


### References


1. M.L. Griffith, D.M. Keicher, C.L. Atwood, J.A. Romero, J.E. Smugeresky, L.D. Harwell, and D.L. Greene, *Proceedings of the Solid Freeform Fabrication Symposium*, Austin, TX, (1996), pp. 125-131.
2. M.L. Griffith, M.E. Schlienger, L.D. Harwell, M.S. Oliver, M.D. Baldwin, M.T. Ensz, M. Essien, J. Brooks, C.V. Robino, J.E. Smugeresky, W.H. Hofmeister, M.J. Wert, and D.V. Nelson, *Materials and Design*, 20, 107-113, (1999).
3. W. Hofmeister, M. Wert, J. Smugeresky, J.A. Philliber, M. Griffith, and M. Ensz, *JOM*, Vol. 51, No. 7, pp. (1999).
4. A. Vasinonta, J. Beuth, and M. Griffith, *Proceedings of the Solid Freeform Fabrication Symposium*, Austin, TX, (1999), pp. 383-391.
5. C.A. Brice, K.I. Schwendner, D.W. Mahaffey, E.H. Moore, and H.L. Fraser, *Proceedings of the Solid Freeform Fabrication Symposium*, Austin, TX, (1999), pp. 369-374.
6. J. Brooks, C. Robino, T. Headley, S. Goods, and M. Griffith, *Proceedings of the Solid Freeform Fabrication Symposium*, Austin, TX, (1999), pp. 375-382.
7. R. M. German, *Powder Metallurgy Science*, Metal Powder Industries Federation, Princeton, NJ, (1984).
8. B.H. Rabin, G.R. Smolik, and G.E. Korth, *Mat. Sci. and Eng. A*, A124, (1990), 1-7.
9. J.C. Russ, *Practical Stereology*, Plenum Press, New York, NY, (1986), pp. 53-72.